

Effect of debris damming on wave-induced hydrodynamic loads against free-standing buildings with openings

Wüthrich, Davide; Ylla Arbós, Clàudia; Pfister, Michael; Schleiss, Anton J.

DOI

[10.1061/\(ASCE\)WW.1943-5460.0000541](https://doi.org/10.1061/(ASCE)WW.1943-5460.0000541)

Publication date

2020

Document Version

Accepted author manuscript

Published in

Journal of Waterway, Port, Coastal and Ocean Engineering

Citation (APA)

Wüthrich, D., Ylla Arbós, C., Pfister, M., & Schleiss, A. J. (2020). Effect of debris damming on wave-induced hydrodynamic loads against free-standing buildings with openings. *Journal of Waterway, Port, Coastal and Ocean Engineering*, 146(1), Article 04019036. [https://doi.org/10.1061/\(ASCE\)WW.1943-5460.0000541](https://doi.org/10.1061/(ASCE)WW.1943-5460.0000541)

Important note

To cite this publication, please use the final published version (if applicable). Please check the document version above.

Copyright

Other than for strictly personal use, it is not permitted to download, forward or distribute the text or part of it, without the consent of the author(s) and/or copyright holder(s), unless the work is under an open content license such as Creative Commons.

Takedown policy

Please contact us and provide details if you believe this document breaches copyrights. We will remove access to the work immediately and investigate your claim.

1 EFFECT OF DEBRIS DAMMING ON WAVE-INDUCED
2 HYDRODYNAMIC LOADS AGAINST FREE-STANDING
3 BUILDINGS WITH OPENINGS

4 Davide WÜTHRICH, Postdoctoral researcher (corresponding author)
5 Laboratory of Hydraulic Constructions (LCH), Ecole Polytechnique Fédérale de Lausanne (EPFL),
6 ENAC, Station 18, 1015 Lausanne, Switzerland, currently at School of Civil Engineering, The
7 University of Queensland, Brisbane, QLD 4072, Australia (d.wuthrich@uq.edu.au)

8 Clàudia YLLA ARBÓS, PhD Student
9 Laboratory of Hydraulic Constructions (LCH), Ecole Polytechnique Fédérale de Lausanne (EPFL),
10 ENAC, Station 18, 1015 Lausanne, Switzerland, currently at Department of Hydraulic Engineering, TU
11 Delft, Netherlands (c.yllaarbos@tudelft.nl)

12 Michael PFISTER, Professor
13 Civil Engineering Department, Haute Ecole d'Ingénierie et d'Architecture de Fribourg (HEIA-FR, HES-
14 SO), 1705 Fribourg, Switzerland (michael.pfister@hefr.ch)

15 Anton J. SCHLEISS, Professor
16 Laboratory of Hydraulic Constructions (LCH), Ecole Polytechnique Fédérale de Lausanne (EPFL),
17 ENAC, Station 18, 1015 Lausanne, Switzerland (anton.schleiss@epfl.ch)

18

19 *This material may be found at <https://ascelibrary.org/doi/abs/10.1061/%28ASCE%29WW.1943-5460.0000541>".*

21

22 **Abstract**

23 Tsunamis, impulse waves and dam-break waves are rare but catastrophic events, associated with
24 casualties and damages to infrastructures. An adequate description of these waves is vital to assure
25 human safety and generate resilient structures. Furthermore, a specific building geometry with openings,
26 such as windows and doors, reduces wave-induced loads and increases the probability that a building
27 withstands. However, waves often carry a large volume of debris, generating supplementary impact
28 forces and creating “debris-dams” around buildings, thus limiting the beneficial effects of the openings.
29 Herein, a preliminary study on the 3D effect of debris-dams on the post-peak wave-induced loads under
30 unsteady flow conditions is presented based on laboratory experiments. Both wooden logs (forest) and
31 shipping containers were tested, showing a different behavior. Shipping containers were associated with
32 severe impact force peaks, whereas the interlocking nature of forest-type debris provoked a compact
33 “debris dam” leading to higher and longer-lasting hydrodynamic forces. The arrangement of the debris

34 also had an influence on the resulting structural loading. All tested scenarios were analyzed in terms of
35 horizontal forces, cantilever arm and impulse acting on the building. This study presents a methodology
36 to support the evaluation of post-peak debris-induced loads for the design of safer resilient buildings.

37 **Key words:** Unsteady flows, Tsunami, Debris-dam, Debris loads, Structural loading.

38 **Introduction**

39 Tsunamis are unsteady flows, generated in the ocean, that propagate inland. In mountain environments,
40 similar inland flows are generated by landslides penetrating into water reservoirs (impulse waves) and
41 dam-break waves. These phenomena are rare, but have the ability to cause destruction and devastation
42 along their path, damaging critical infrastructures and endangering people's lives (Fritz et al. 2011;
43 Chock et al. 2012). The 1963 Vajont impulse wave, the 2004 Indian Ocean tsunami, and the 2011
44 Tohoku Japan tsunami are examples of such destructive power. However, these events showed that
45 measures are possible to reduce casualties and damages to critical infrastructures.

46 The generation, propagation and impact of highly unsteady inland flows such as tsunamis, impulse
47 waves and dam-break waves were widely investigated in the past. Chanson (2006) showed that tsunamis
48 propagating inland could be reproduced using the Ritter (1892) solution for a dam-break wave. The
49 impact of such waves on impervious free-standing buildings was the object of a number of research
50 projects, providing engineers with tools to design resistant infrastructures. Triatmadja and Nurhasanah
51 (2012) focused on the effect of openings in the building, and Wüthrich et al. (2018b) showed that a flow
52 through the buildings resulted into lower wave-induced forces and reduced inundation depths.

53 However, post-event field surveys showed that tsunami waves transport a large amount of debris,
54 responsible for supplementary forces and impulsive destruction (Saatcioglu et al. 2005, Robertson et al.
55 2007, Takahashi et al. 2010).

56 In addition, a certain quantity of debris remains trapped at the building, creating a "debris-dam" in and
57 around the structure, thus limiting the beneficial effect of openings. Bocchiola et al. (2008) conducted
58 an early study on the formation of the "debris-dam". Given the complexity of the phenomenon and the
59 processes involved, several studies have addressed the issue of debris motion (Matsutomi 2009, Yeom

60 et al. 2009, Rueben et al. 2015, Shafiei et al. 2016). Naito et al. (2013) provided a classification of the
61 debris while studying its motion on coastal areas, and compared it to the 2011 Tohoku tsunami. Nistor
62 et al. (2016) experimentally investigated the trajectory of shipping containers over a horizontal channel,
63 showing that the spreading angle was a function of the number of containers. Stolle et al. (2018c)
64 observed that hydraulic conditions had a significant influence on the debris trajectory, with larger
65 impoundment depths generating lesser lateral spreading. Goseberg et al. (2016a) focused on the debris
66 motion through fixed obstacles under unsteady flow conditions.

67 The additional forces generated by the impact of debris on coastal structures was analyzed by Haehnel
68 and Daly (2004), Matsutomi (2009), Nistor et al. (2011, 2017) and most recently Derschum et al. (2018)
69 and Stolle et al. (2018a). The formation of a “debris dam” around bridge piers during flood events was
70 investigated by Parola (2000) and by Stolle et al. (2017b) under 2D steady flow conditions. Pasha and
71 Tanaka (2016) focused on the capture of debris at inland forests, pointing out that different debris shapes
72 led to different damming behaviors. Most recently, the issue of debris dams under 2-dimensional
73 unsteady flow conditions was addressed by Stolle et al. (2018b) for a number of mixtures composed of
74 shipping containers, boards and hydro poles. This study also showed that the presence of a recirculating
75 roller generated a more dynamic debris dam, leading to lower retention coefficients when compared to
76 the steady state case.

77 In alpine environments, the accumulation and the dynamics of debris on river dams and spillways were
78 investigated by Pfister et al. (2013) and Furlan et al. (2018), among others. Schmocker and Hager (2013)
79 reported that the accumulation of debris upstream of debris rack generated an obstruction of the flow,
80 leading to an increase in the upstream water level.

81 Despite these major contributions, the effect of a “debris dam” under 3-dimensional, rapidly-varied
82 unsteady flow conditions was so far rarely addressed and the induced loads remain difficult to assess.

83 In addition, except for the recent contribution of Stolle et al. (2018b), most previous studies only focused
84 on one type of debris and the behavior of mixtures with different debris shapes and sizes has not been
85 analyzed. In line with the research conducted by Wüthrich et al. (2018b) for free-standing buildings with
86 openings, the present work investigates the effect of two types of debris on the resulting loads exerted

87 on a free-standing building with openings. Particular attention is given to the post-peak hydrodynamic
88 forces induced by the accumulation of debris in front of the openings. More specifically, this study:

- 89 • visually assesses the behavior of two types of debris (shipping containers and wooden logs) for
90 different initial volumes.
- 91 • analyses the effect of a 3D, initially supercritical, flow and debris accumulation on a free-standing
92 building with a surface porosity of 60%.
- 93 • quantifies loads induced by the debris in terms of horizontal forces, cantilever arm and impulse.

94 **Experimental Set-up**

95 This work is based on an experimental approach and the set-up is shown in Figure 1. A single surge
96 propagating over a dry horizontal bed was generated using a vertical release technique (Wüthrich et al.
97 2018a), reproducing tsunami-like flows propagating inland. The channel had a length of 14 m and a
98 width of $W = 1.4$ m. The dry bed surge propagated on a horizontal, smooth channel with a front celerity
99 $U = 2.35$ m/s and a maximum inundation depth $h_{\max} = 0.13$ m. If a geometric scale factor of 1:30 is
100 assumed, these values corresponded to common values observed during past tsunamis, during which
101 Froude numbers $Fr = U/(gh)^{0.5} \sim 1$ were reported (Chock et al. 2012, Fritz et al. 2011). In addition, flow
102 depths of 4 to 7 m were measured in the southern part of Khao Lak, Thailand, during the 2004 Indian
103 Ocean tsunami (Dias et al. 2006) and velocities up to 10 to 13 m/s near the Sendai Airport during the
104 2011 Tōhoku, Japan, tsunami (Jaffe et al. 2012).

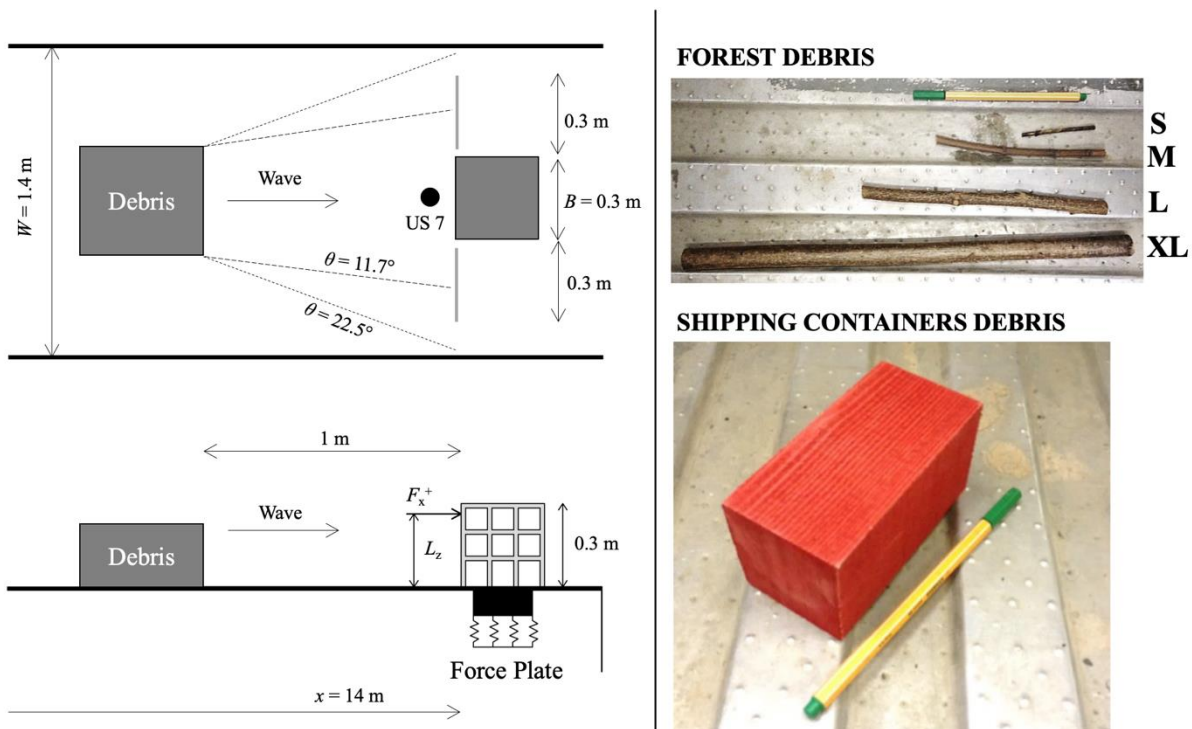
105 A building was inserted in the channel, consisting of an aluminum cube of $B = 0.3 \times 0.3 \times 0.3$ m side
106 length, representing a three-floor residential house. Push-over tests showed Eigen frequencies of 43.8
107 Hz in the x -direction and 46.4 Hz in the y -direction; more details can be found in Wüthrich (2018).
108 Herein, the building had a total front surface porosity $P = 60\%$, uniformly distributed over its height.
109 Two additional transversal porous fronts were added, resulting into a blockage ratio of $\beta = W/3B = 1.56$
110 (Figure 1). Note that these fronts only increased the blockage ratio, but were not connected to the central
111 building nor to the measuring force plate.

112 Shipping containers and debris from the forest environment were reproduced herein. The wooden
 113 parallelepipeds simulate shipping containers (index C) commonly stored in coastal areas subject to
 114 tsunami hazard. These had model dimension of $0.058 \times 0.058 \times 0.120$ m, which corresponded to prototype
 115 values of $1.74 \times 1.74 \times 3.6$ m for a 1:30 geometric scaling ratio, with similar values to those used by
 116 Goseberg et al. (2016b). For a density $\rho = 502 \text{ kg/m}^3$, this reproduced half-full containers of 5.5 tons.
 117 These values are within the range of containers temporarily stored in coastal areas (Aghl et al. 2015).
 118 The forest debris (index F) contains poles and large wooden logs of different lengths L . The details of
 119 the debris are given in Figure 1 and Table 1. The densities of these objects ranged between $\rho = 507$ and
 120 717 kg/m^3 , therefore being positively buoyant. This is in agreement with the values used by Stolle et al.
 121 (2017b) for similar studies. According to the classification by Naito et al. (2013) these objects
 122 correspond to “moderate debris” at prototype level.

123 Table 1 – Physical characteristics of the debris (model scale values)

Type		Length L [m]	Diameter / Width [m]	Density [kg/m^3]
Forest	Small (S)	0.0662	0.0033	507
	Medium (M)	0.1656	0.0071	607
	Large (L)	0.2337	0.0120	565
	Extra Large (XL)	0.4300	0.0180	717
Shipping container		0.1200	0.0580	502

124

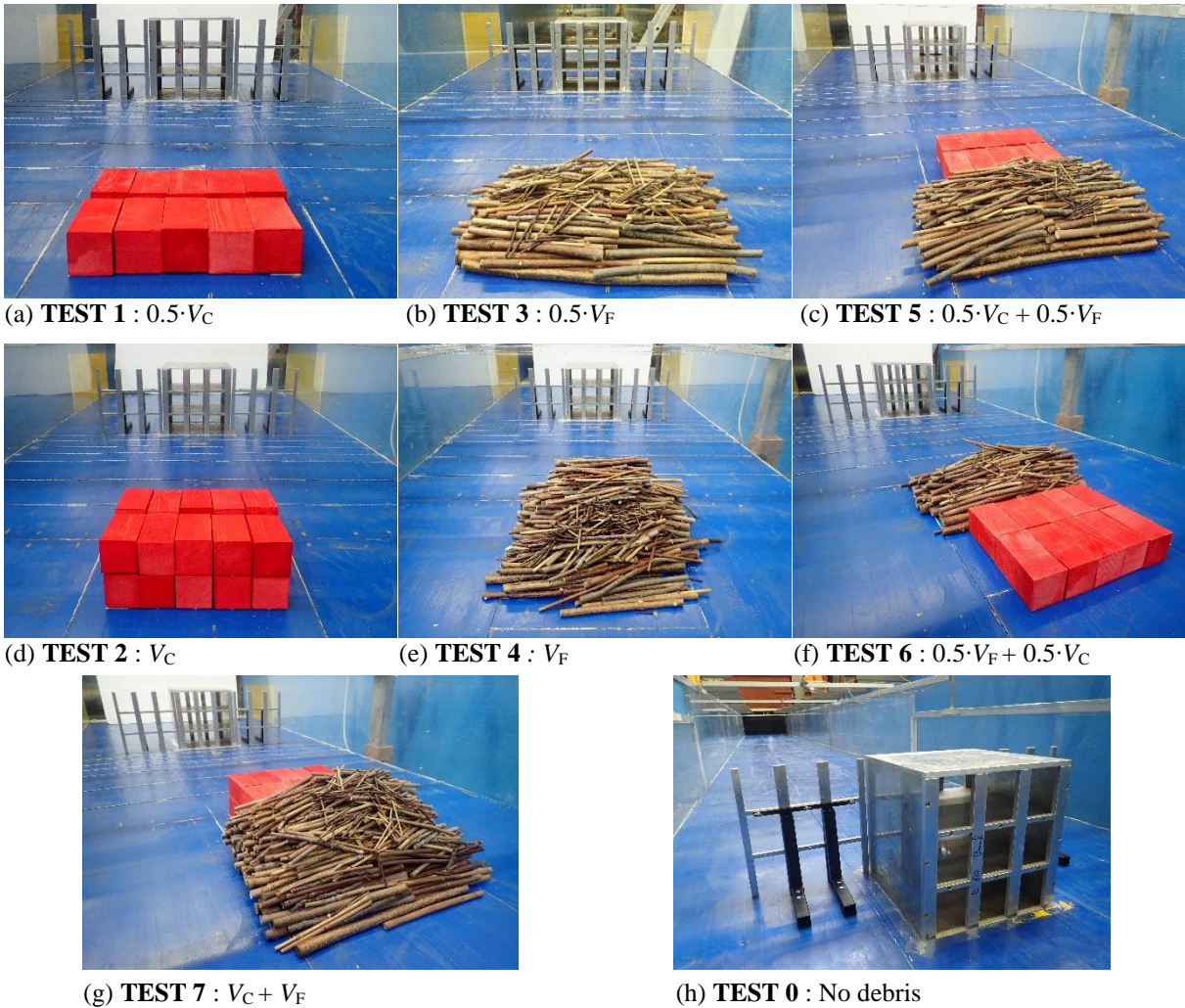


125

Figure 1 – Experimental set-up and debris characteristics (model scale values).

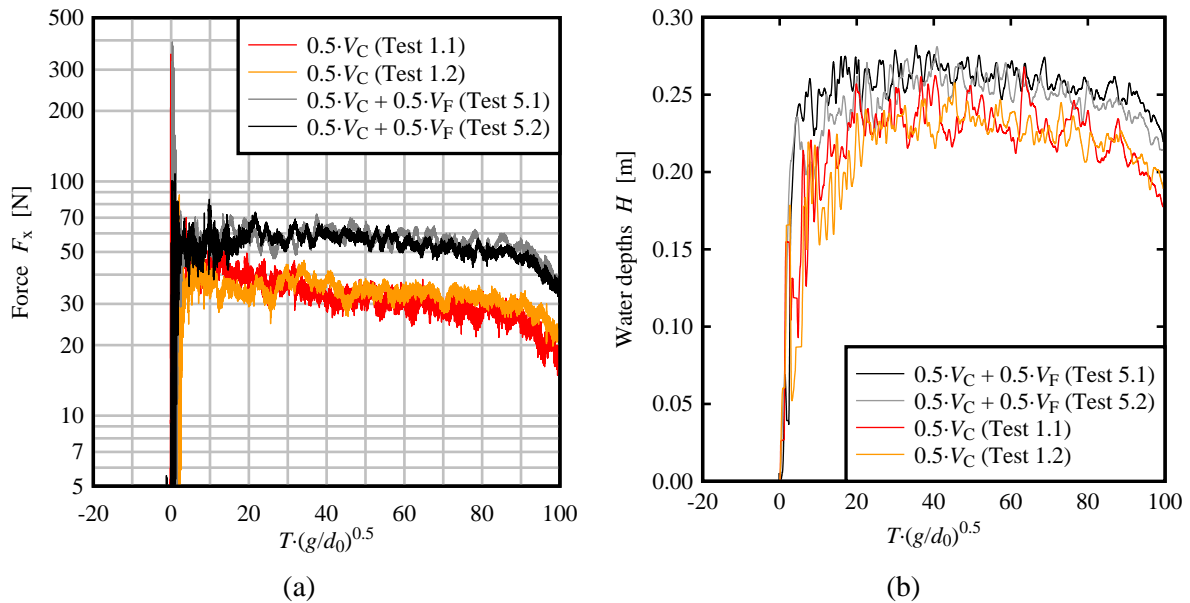
126
127
128 Seven debris configurations (Tests 1 to 7) were tested, as shown in Figure 2. The debris was inserted in
129 the middle of the channel at a distance of 1 m upstream from the building, over a width of 0.30 to 0.40
130 m (Figure 1). Stolle et al. (2018c) showed that a distance of 0.75 m was sufficient to guarantee full
131 acceleration of containers with comparable size and similar flow conditions. Naito et al. (2013) found a
132 spreading angle of $\theta = \pm 22.5^\circ$ for general debris transported during tsunami events. More recently, Nistor
133 et al. (2016) showed that containers on a smooth horizontal bed propagated with an angle affected by
134 the number of debris, leading to $\theta = \pm 19.7^\circ$ for 20 containers (maximum value allocated during Test 2)
135 and $\theta = \pm 11.7^\circ$ for 10 containers (minimum value allocated during Test 1). Hence, the disposition used
136 herein guaranteed that the central building (where forces are measured) was included within the debris
137 trajectory for all spreading angles (Figure 1). For the configuration with 10 containers, a portion of the
138 additional sides was located outside the debris trajectory, however the generation of a dam in front of
139 the central structure remained guaranteed.

140 The standard debris volume was $V = 0.0081 \text{ m}^3$ (model scale), which corresponded to 1/3 of the total
141 building volume. Schmocker and Hager (2013) used a similar approach. Furthermore, the chosen
142 volume corresponded to a number of 20 shipping containers, commonly stored on coastlines subject to
143 tsunami hazards, and consistent with Nistor et al. (2016) who used a maximum number of 18 containers.
144 The characteristic distribution of the forest debris was chosen based on a flood-related survey executed
145 by Bezzola and Hegg (2007) and shown in Figure 8a. All debris configurations were related to the
146 reference scenario without debris (Test 0). All experiments were conducted on a dry channel bed, which
147 corresponded to the conditions encountered during the first tsunami wave, assumed to be the one
148 transporting the largest debris volume. Note that a minimum of 24 hours was ensured between
149 consecutive tests to ensure that both the debris and the channel were dry. For the Tests 5 and 6, the order
150 of the containers and forest debris was switched, but the volumes remained identical. A configuration
151 with a double volume of debris ($2V$), including both containers and forest, was also tested (Test 7).



152 Figure 2 – Configurations tested: (a) Test 1 with $0.5V_C$ containers, (b) Test 3 with $0.5V_F$ forest debris, (c) Test 5
 153 with $0.5V_C + 0.5V_F$ containers and forest debris, (d) Test 2 with V_C containers, (e) Test 4 with V_C forest debris,
 154 (f) Test 6 with $0.5V_F + 0.5V_C$ forest debris and containers, (g) Test 7 with $V_F + V_C$ forest debris and containers,
 155 and (h) Test 0 without debris (view from downstream).

156 The repeatability of the tests was confirmed for two configurations with shipping containers and forest
 157 debris (Test 1 and 5 in Figure 2). The loading processes for both tests is detailed in Figure 3a. Although
 158 some punctual disagreement can be observed for the peak impact forces, results show good repeatability
 159 in the post-peak hydrodynamic phase, which is the focus of the present study. Despite the oscillations
 160 due to the presence of the roller on the upstream side of the building, Figure 3b also shows a similar
 161 behavior of the upstream water depths for each repetition.



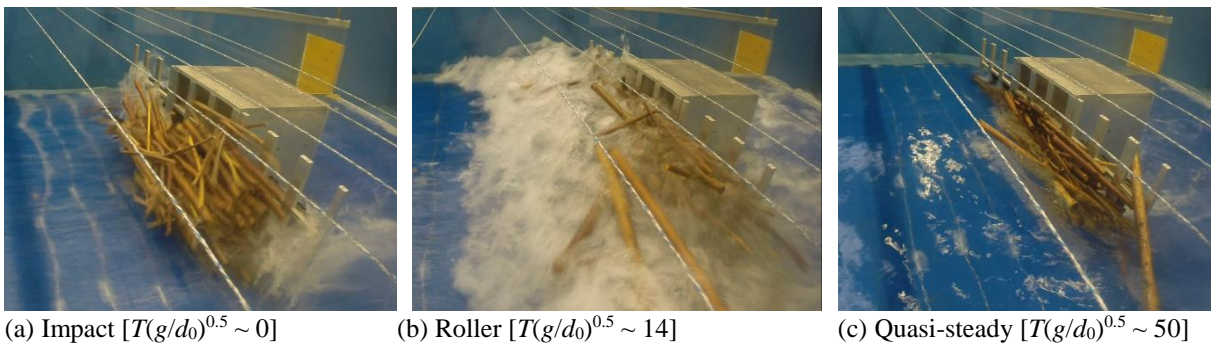
162 Figure 3 – Repeatability of the tests for both shipping containers ($0.5V_C$, Test 1) and a mixture of containers and
 163 forest debris ($0.5 \cdot V_C + 0.5 \cdot V_F$, Test 5) in terms of (a) horizontal forces F_x and (b) upstream water depths H .
 164 (values at model scale)

165 A Force Plate (AMTI MC6-1000) was fixed under the building to measure forces and moments acting
 166 on the building with a frequency of 2 kHz. Two video cameras were placed at about 0.5 and 1.5 m
 167 upstream of the structure, following the debris with a rate of 29 fps. The reference coordinate system
 168 for the forces is introduced in Figure 1. The water level 0.015 m upstream of the structure (US7) was
 169 recorded using an Ultrasonic distance Sensors (US), type Baumer UNAM 30I6103, with a measuring
 170 range from 0.1 to 1.0 m. This was sampled with an accuracy of 0.5 mm and a response time of less than
 171 80 ms, leading to an acquisition frequency of 12.5 Hz.

172 **Blocking process**

173 The tested dry bed surges were identical for all tests ($h_{\max} = 0.13$ m, $U = 2.35$ m/s), only the debris
 174 configuration changed. The propagating surges mobilized the inserted debris, transporting it onto the
 175 building. A temporal evolution of the dam formation for Test 3 is detailed in Figure 4. It was noted that
 176 not all debris collided with the building simultaneously, and that the very first impact was mostly
 177 produced by only a few objects (Figure 4a). After this initial impact, a portion of the debris remained
 178 attached to the structure forming a “debris dam”, while the 3-dimensional set-up allowed for some debris
 179 to flow around the building. During this process, a turbulent aerated and recirculating roller occurred on
 180 the upstream front of the building, as shown in Figure 4b and Figure 5 for Tests 2 and 4. A video analysis

181 showed that a roller extended over 0.3 to 0.5 m upstream of the building front, with a strong fluctuating
182 nature. A simple FFT analysis of the water depth measured by the US sensor located above the roller
183 revealed dominant roller frequencies around 1-1.5 Hz for all tested configurations. During the
184 recirculation, some debris remained constantly attached to the building, whereas some others were
185 incorporated in the recirculating roller, thus constantly modifying the “debris-dam” acting on the
186 building. This phenomenon was more evident for the forest debris as suggested by Figure 5b. The 3-
187 dimensional nature of the flow and the streamlines around the building allowed for some debris to be
188 washed away, as shown in Figure 5a.



189 Figure 4 – Temporal evolution of the debris dam for Test 3 with $0.5 \cdot V_F$ forest debris.

190 Video processing and visual tracking of the debris during the impact showed that ~70 to 80% of the
191 non-retained containers were washed away in the first second after the impact (model scale). The
192 remaining 20% remained initially caught in the roller, slowly bouncing towards the side of the building,
193 until it reaches the edge. Because of the high number and diversity of the logs, similar considerations
194 cannot be drawn for the forest debris. The debris “trapped” within the recirculating roller reduced the
195 discharge flowing through the openings of the building, hence increasing the water depth H at the
196 upstream front of the building. This is in agreement with the findings of Schmocker and Hager (2013)
197 and Stolle et al. (2017a, 2018b). Due to the constriction of the flow, the upstream Froude number
198 decreased, and the propagating roller disappeared, generating a quasi-steady clear water flow around the
199 building. The newly formed debris dam became visible after the disappearance of the roller (Figure 4c).
200 At this stage, the subcritical flow through the openings pushes the debris against the building and no
201 relevant modification of the debris is observed during the decreasing part of the wave.

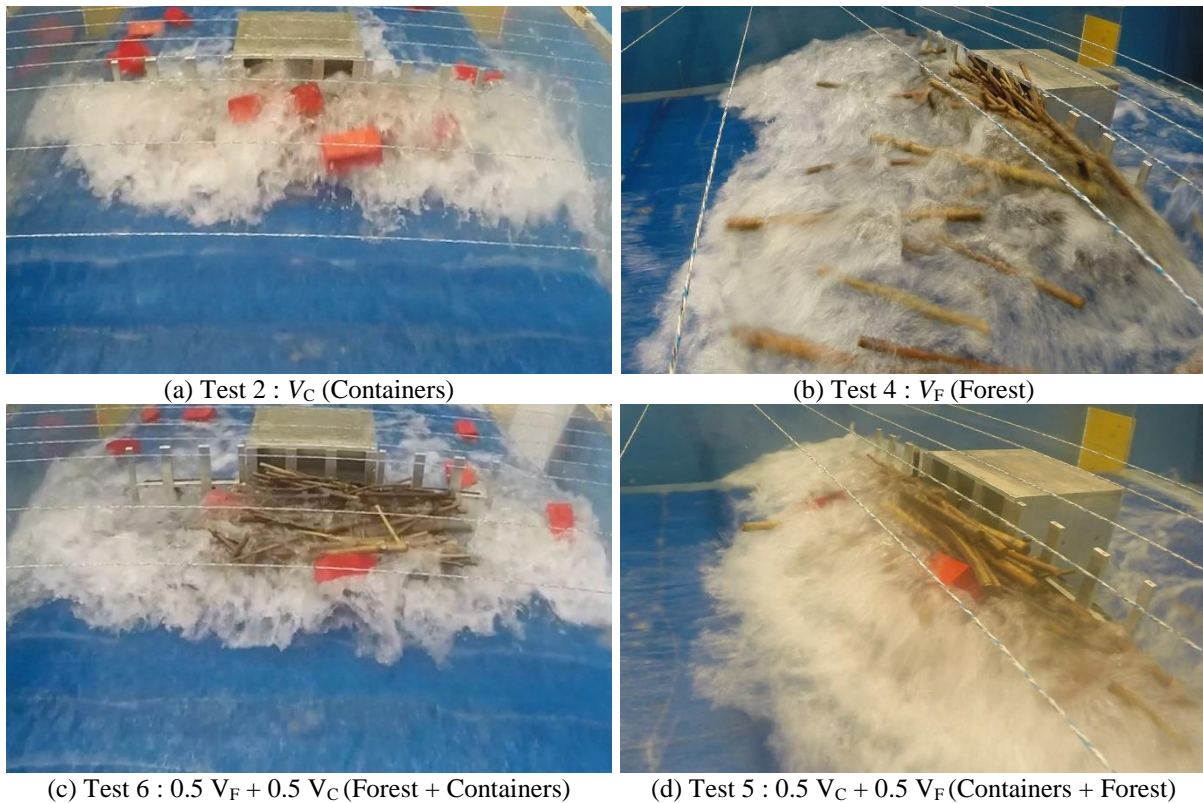
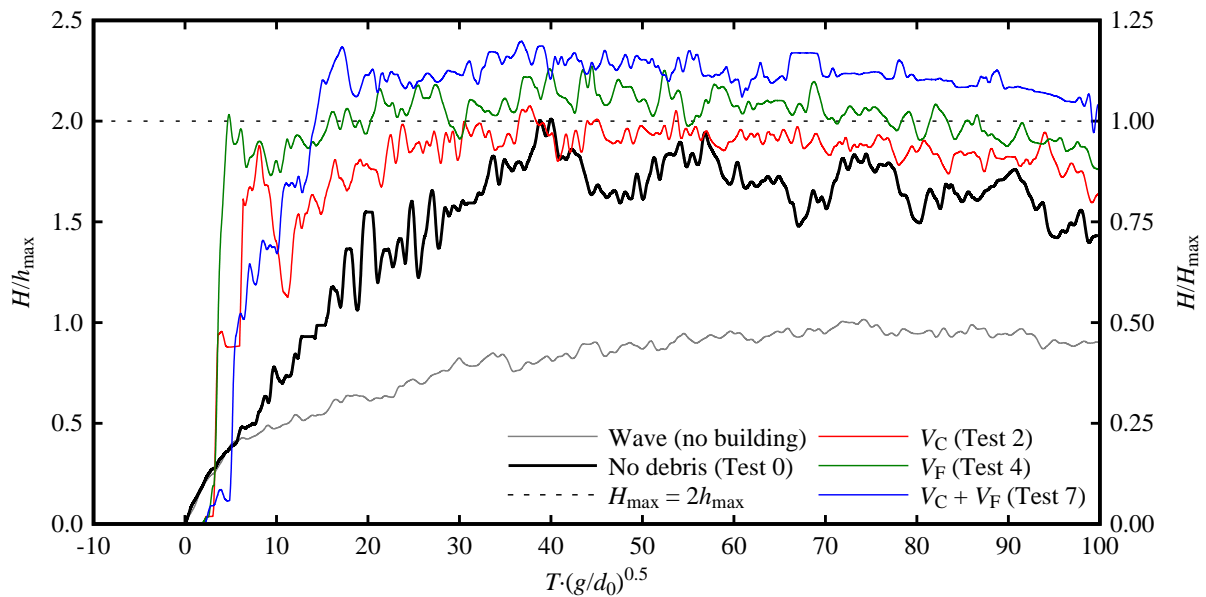


Figure 5 – Specific features of the unsteady flow and the recirculating roller during the generation of the debris dam.

202
 203
 204 The upstream increase in water depth was captured by the US sensor and the time development is
 205 presented in Figure 6. Time T is normalized using the gravity constant $g = 9.81 \text{ m/s}^2$ and the equivalent
 206 impoundment depth d_0 , in line with Wüthrich et al. (2018a). $T = 0$ is set when the wave impacts against
 207 the building. The water depths upstream of the building were recorded using an Ultrasonic distance
 208 Sensor (US), capturing the flow depth averaged on a surface of 0.011 m^2 for a duration of 80 ms. Please
 209 note that the delay in arrival time in Figure 6 is due to the presence of the debris within the channel,
 210 acting as an obstacle to the propagating wave. Although the measurements are affected by aeration and
 211 splashes of the recirculating roller, these clearly show increased values of the water depth H (with the
 212 building) up to 2 to 2.5 times the maximum wave height h_{\max} without the building. As shown in Figure
 213 6, these water depths (with building and debris) were 20 to 22% higher than those recorded without the
 214 presence of debris in the flow. The highest water depths corresponded to the test with the largest debris
 215 volume ($2V$, Test 7). For an equal debris volume V , the tests with forest debris generated higher water
 216 depths as compared to the containers. It is important to point out that higher water depths due to the

217 presence of the debris lead to a higher probability of building overtopping and thus less secure vertical
 218 shelters.



219
 220 Figure 6 – Upstream water depths H with building, measured at 0.15 m upstream from the latter, where $h_{\max} =$
 221 0.13 m is the maximum water depth without the structure, and $H_{\max} = 0.26$ m the maximum water depth with the
 222 structure and no debris (Test 0).

223 Figure 2 showed the initial debris configurations, whereas the dispositions after the wave passed are
 224 shown in Figure 7. The debris volume remaining in front of the building was determined after each test
 225 and a retention coefficient B_{eff} was defined as the ratio between the retained volume and the total inserted
 226 volume. Results are detailed in Table 2, showing an overall retention coefficient of 58% for the forest
 227 debris (Test 3 and 4), compared to an average coefficient of 47.5% for the containers (Test 1 with 45%
 228 and 2 with 50%). This difference is attributed to the higher tendency of the forest debris to interlock,
 229 creating a more solid “debris-dam”. It is interesting to point out that for both containers and forest
 230 similar retention coefficients were found for different initial volumes (Test 1, 2, and Test 3, 4).



(a) TEST 1 : $0.5 \cdot V_C$

(b) TEST 3 : $0.5 \cdot V_F$

(c) TEST 5 : $0.5 \cdot V_C + 0.5 \cdot V_F$



(d) **TEST 2** : V_C

(e) **TEST 4** : V_F

(f) **TEST 6** : $0.5 \cdot V_F + 0.5 \cdot V_C$



(g) **TEST 7** : $V_C + V_F$

231 Figure 7 – Disposition of the debris after the wave: (a) Test 1 with $0.5V_C$ containers, (b) Test 3 with $0.5V_F$ forest
 232 debris, (c) Test 5 with $0.5V_C + 0.5V_F$ containers and forest debris, (d) Test 2 with V_C containers, (e) Test 4 with
 233 V_C forest debris, (f) Test 6 with $0.5V_F + 0.5V_C$ forest debris and containers, (g) Test 7 with $V_F + V_C$ forest
 234 debris and containers.

235 Tests 5 and 6 had both the standard debris volume V , but the order of insertion was reversed (Figure 2c
 236 and f). Observations showed that less containers accumulates in front of the building if the logs are
 237 located upstream of the containers (Test 6, Figure 6c). This is because the “debris dam” formed by the
 238 logs acts as protection, such that the containers are washed away by the flow. Contrarily, if the shipping
 239 containers are located upstream of the logs, the interlocking nature of the forest debris has a tendency
 240 to incorporate the containers within the newly formed “debris-dam”, thus generating a larger
 241 accumulation and a higher retention coefficient B_{eff} (Test 5, Figure 6f).

242 This point was confirmed by the configuration with $2V$ (Test 7) in Figure 7g, where one can notice the
 243 large amount of containers integrated within the “debris dam”. These results are in agreement with the
 244 findings of Bocchiola et al. (2008) and Stolle et al. (2017b), pointing out the importance of the first
 245 object caught in the formation of the “debris dam” (“key” log). These results show that containers should
 246 be stored further away from the building if the formation of the “debris-dam” shall be limited.

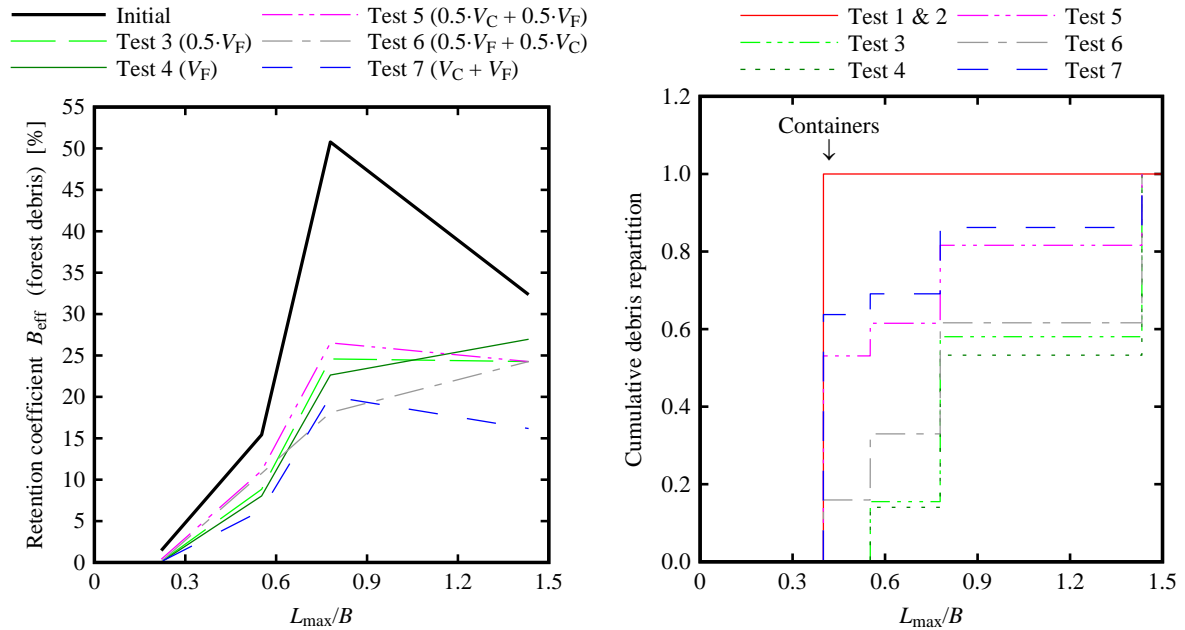
247 Videos and post-tests observations showed that the horizontal foot-print of the debris dams was
 248 distributed on the entire structure width.

249 Table 2 – Detailed on the retained volume and the “debris dam” ($V = 0.0081 \text{ m}^3$)

	Configuration	Total volume retention coefficient [%]	Containers volume retention coefficient [%]	Forest volume retention coefficient [%]	Retained debris volume per building width [cm^3/cm]
Test 1	$0.5 V_C$	45%	45%	-	22.43
Test 2	V_C	50%	50%	-	44.85
Test 3	$0.5 V_F$	58%	-	58%	26.07
Test 4	V_F	58%	-	58%	52.04
Test 5	$0.5 V_C + 0.5 V_F$	66%	70%	62%	59.48
Test 6	$0.5 V_F + 0.5 V_C$	32%	10%	53%	28.51
Test 7	$V_C + V_F$	59%	75%	43%	105.70

250 Details on the retained volumes for both containers and forest debris are presented in Table 2. In
251 addition, Figure 8 provides details on physical characteristics of the “debris dam” formed in front of the
252 building. These were derived from the remaining debris after the wave (Figure 7). Figure 8a presents
253 the retention coefficient (B_{eff}) for the forest debris with different sizes, comparing it with the total initial
254 distribution. Debris are classified in terms of their characteristic length, herein defined as the maximum
255 length L_{max} . Results show a higher retention coefficient for forest debris with longer characteristic length,
256 in agreement with the findings of Pfister et al. (2013) and Pasha and Tanaka (2016). For all tests, the
257 retention coefficient of medium size logs seems to be constantly larger than the values reported by Stolle
258 et al. (2018b) for hydro poles (12 cm, $B_{\text{eff}} = 8.6\%$), thus suggesting the importance of the interlocking
259 nature between debris with different sizes, increasing the retention coefficient. The different nature of
260 the debris trapped within the dam is reflected in the cumulative percentage of debris (containers and
261 forest debris) presented in the Figure 8b. This results into different physical properties of the dam,
262 leading to different load conditions.

263 The 3-dimensional nature of the flow around the building allowed for some debris to be washed away
264 and is thus responsible for the lower values of B_{eff} as compared to Stolle et al. (2018b) for a 2-dimensional
265 unsteady flow condition. This is especially true for shipping containers, for which Stolle et al. (2017a,
266 2018b) reported retention coefficient of 94.6% and 73.6% for steady and unsteady flows, respectively,
267 compared to the 50% found in this study.



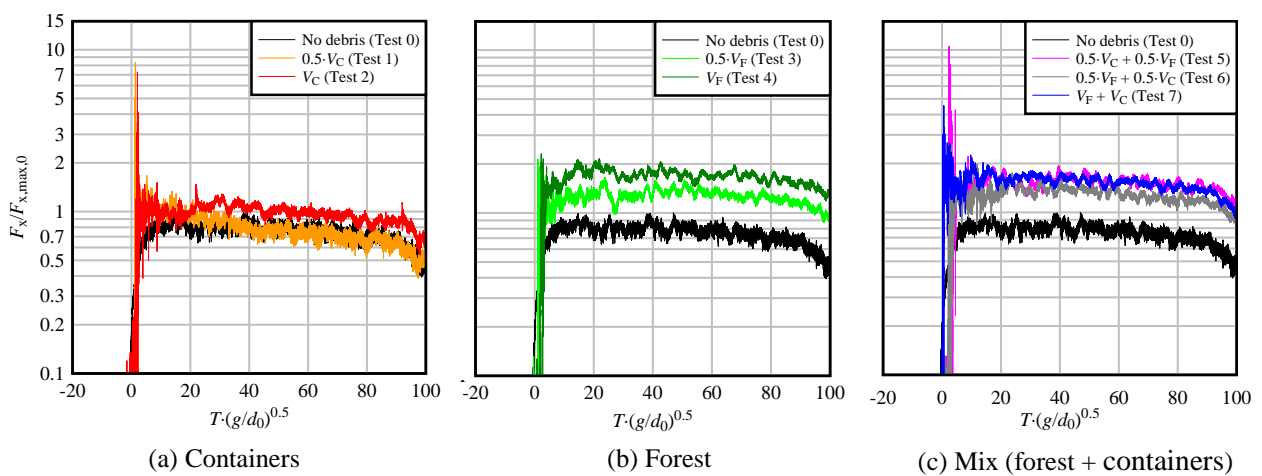
268 Figure 8 – Physical properties of the debris dam formed upstream of the building: (a) Forest retention
 269 coefficients ($B_{\text{eff}} = V_{\text{retained}}/V_{\text{total}}$); (b) cumulative debris repartition. L_{max} is normalised using the central
 270 building width ($B = 0.3$ m)

271 Structural loading

272 The presence of debris within the flow modified the structural loading as compared to that of “pure”
 273 water waves described by Wüthrich et al. (2018b) for identical buildings (with openings). As shown in
 274 Figure 9, the arrival of the wave is characterized by initial *impact forces*, followed by a more constant
 275 and sustained load, herein identified as the *hydrodynamic force*, in line with Yeh et al. (2015). Note that
 276 no pronounced impact force was recorded for the reference scenario without debris (Test 0). The peak
 277 impact forces measured for debris relate to their abrupt impact and an instantaneous momentum transfer.
 278 Pure water (Test 0) transfers impulse over time visualized as a hydrodynamic force in the data. All forces
 279 are normalized using the maximum measured force for Test 0 without debris ($F_{x,\text{max},0} = 37.17$ N).

280 The loading process showed different characteristics according to the type of debris. These are presented
 281 in Figure 9a on a logarithmic scale. Containers were characterized by high impact forces reaching up to
 282 8-10 times the maximum horizontal reference force $F_{x,\text{max},0}$ (measured without debris, Test 0). The
 283 magnitude of impact forces were in line with the values suggested by FEMA 55 (2011) and ASCE7-06
 284 (2016) for design purposes, however the peak impact forces do not represent the object of this study.
 285 After a small transition phase characterized by a ‘*resettlement*’ of the debris (5 to $20 T \cdot (g/d_0)^{0.5}$), the

286 impact phase was followed by a hydrodynamic phase with a behavior similar to the configuration
 287 without debris. This is attributed to the non-interlocking and porous nature of containers, thus limiting
 288 the formation of a coherent “debris-dam” in front of the building. Contrarily to shipping containers, the
 289 *forest debris* showed limited impact forces, whereas the post-peak hydrodynamic force was almost twice
 290 that induced by the wave without debris (Figure 9b). This increase in post-peak hydrodynamic force is
 291 attributed to the formation of a “debris-dam” in front of the porous building, blocking some of the
 292 openings, as previously shown in Figure 5 and implicitly in Figure 7. This leads to higher hydrodynamic
 293 forces acting on the building for a relatively long time interval.



294 Figure 9 – Forces measured for the configuration with and without debris: (a) containers; (b) forest debris; (c)
 295 mix (forest + containers).

296 For the same volume V , two configurations including both containers and forest debris were tested, with
 297 a reversed order (Tests 5 and 6, Figure 2 and 5c). This influenced the building load, combining features
 298 of the individual configurations (Tests 2 and 4). An important impact force is observed for the
 299 configuration with forest debris upstream and containers downstream, thus closer to the building (Test
 300 5, Figure 2 and Figure 9c) because of the direct impact of the containers on the building. Subsequently,
 301 the wooden logs upstream of the containers generate a “debris-dam” on the upstream side, including
 302 both containers and forest debris. This generated a hydrodynamic force higher than the reference case,
 303 but comparable to the magnitude of the force recorded for the forest debris only (Test 4).

304 The loading process of the configuration with containers upstream and forest debris downstream (Test
 305 6, Figure 2 and Figure 9c) was slightly different. As previously observed for the configuration with
 306 forest debris (Tests 3 and 4) only, the impact of the logs on the building did not generate important

307 impact forces. The formation of the “debris dam” near the building (due to the presence of logs)
308 prevented the direct contact of the containers with the building, and most of the containers were flushed
309 away (Fig. 4f). The formation of the “debris dam” lead again to important hydrodynamic forces.

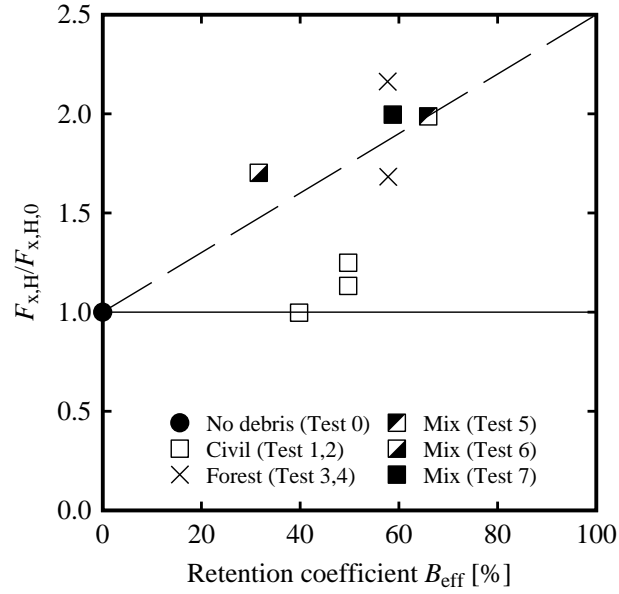
310 This represents an important result, because it shows that the presence of a large amount of forest debris
311 with interlocking properties can partially prevent the direct collision of containers against the building,
312 thus limiting the very high impact forces and subsequent local damages to the structure. However, these
313 forest debris reduce the openings within the building and augment the hydrodynamic force.

314 A representative value of the hydrodynamic (index H) force $F_{x,H}$ was computed as:

$$F_{x,H} = \frac{1}{\Delta T} \int_{20 \cdot \sqrt{\frac{d_0}{g}}}^{80 \cdot \sqrt{\frac{d_0}{g}}} F_x(T) dT \quad [1]$$

315 where the interval 20 to 80 $(d_0/g)^{0.5}$ was chosen herein to focus exclusively on the post-peak
316 hydrodynamic phase. These values $F_{x,H}$ were then normalized with the “pure” water wave $F_{x,H,0}$ force
317 (Test 0) and are presented in Figure 10 as a function of the retention coefficient B_{eff} . The latter was
318 defined as the ratio between the blocked volume and the total supplied volume. One can notice a
319 simplified linear relationship between the retained volume and the increase in hydrodynamic force.
320 These values are shown in Figure 10. Although based on a limited number of experimental tests, this
321 data shows several aspects:

- 322 • Forest (eventually combined with containers) debris highly increases the hydrodynamic force, thus
323 reducing the building porosity.
- 324 • Exclusively containers hardly affect the porosity and thereby the hydrodynamic force.
- 325 • As a first approximation, the correlation between the retention coefficient B_{eff} and the force increase
326 $F_{x,H}/F_{x,H,0}$ can be assumed linear for the configurations including a portion of forest debris.

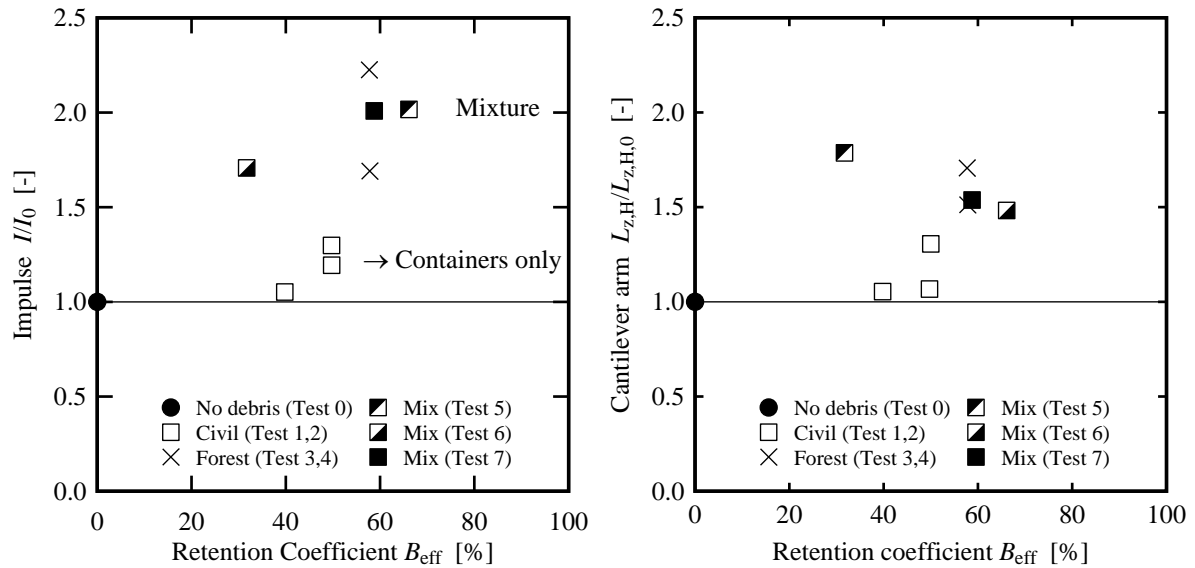


327
 328 Figure 10 – Increase in average hydrodynamic horizontal force $F_{x,H}$ due to the presence of debris in the flow

329
 330 The impulse I transferred from the mixture of water and debris to the building is calculated as the integral
 331 of the force F_x over a given time interval dT as:

$$I = \int_0^{100 \cdot \sqrt{\frac{d_0}{g}}} F_x(T) dT \quad [3]$$

332 where the interval 0 to $100 \cdot (d_0/g)^{0.5}$ was chosen herein as it represented the maximum duration that
 333 allowed to capture the loading process before the decrease of the wave became predominant. The
 334 impulse consideration have the advantage of being less affected by the randomness of the process
 335 compared to peak values (Bullock et al. 2007; Wüthrich et al. 2018b). The normalized impulse is shown
 336 in Figure 11 as a function of the retention coefficient B_{eff} . Furthermore, the impulse is normalized with
 337 the reference test impulse I_0 (Test 0), i.e. the impulse derived from the impacting wave without debris.



338
 339 Figure 11 – Impulse and cantilever arm measured for the configurations with and without debris. All values are
 340 normalized using the impulse and cantilever arm measured for the reference configuration without debris (I_0 ,
 341 $L_{z,0}$, Test 0). [$V = 100\% = 0.008\text{ m}^3$]

342
 343 The consideration of the impulse confirms the previous discussion on the horizontal forces. The presence
 344 of debris augmented also the impulse acting on the building, as compared to the pure water wave (Test
 345 0). For the configuration with exclusively containers, the impulse increase is smaller as compared to the
 346 configuration with an equivalent volume of forest debris. The configurations with a mixture of both
 347 containers and forest debris (Test 5 and 6) show intermediate values. The configuration with the largest
 348 volume (Test 7, 200%) shows no significant increment in total impulse. This is probably a consequence
 349 of the 3-dimensional flow motion around the structure, which limits the formation of the “debris dam”
 350 to a specific volume.

351 The ratio between the moment M_y and the horizontal force F_x gives the cantilever arm $L_z = M_y/F_x$, i.e.
 352 the vertical height at which the force F_x is applied (Figure 1). Similarly to the impulse, the average
 353 values during the hydrodynamic phase are presented in Figure 11b and normalized with $L_{z,H,0}$ as
 354 cantilever arm of Test 0 (no debris) during the hydrodynamic phase. An increase in cantilever arm in
 355 case of formation of a “debris dam” appears. The increase is relatively small for containers ($< 30\%$).
 356 However, it becomes important for forest debris (50-80 %). For the cantilever arm, a dependency on the
 357 debris volume does not clearly emerge from the experimental data. However, a value of around $1.5L_{z,H,0}$
 358 is reached as soon as forest debris are present in the mixture.

359 These results show that the average hydrodynamic forces generated by the “debris dam” are not only
360 greater in magnitude, but also applied at a higher elevation (above $L_{z,H}/L_{z,H,0} = 1$ for the pure water
361 wave), resulting into significantly higher moments acting on the building.

362 **Discussion**

363 This explorative study analyzes the effect of a 3D, initially supercritical, flow and debris accumulation
364 on a free-standing building with openings. Because of the complexity of the process and the number of
365 parameters involved, a number of assumptions made herein can be further discussed.

366 The authors chose to install the debris at a distance of 1 m (model scale) from the building. Although
367 this distance was shown by Stolle et al. (2018c) to be enough to guarantee full acceleration of the
368 shipping containers, this might have affected their trajectory (Nistor et al. 2016), thus influencing the
369 formation of the debris dam and hydrodynamic forces exerted on the building.

370 Another key parameter is the initial volume of debris allocated in the channel. During tsunami events,
371 this value varies with the distance to shoreline, as more debris are entrained during the inland
372 propagation of the flow. Herein two different volumes were tested ($0.5V$ and V), leading to similar
373 retention coefficient, but different volumes within the debris dam (Table 2). Although this study showed
374 a good repeatability, the stochastic and chaotic nature of the debris (Furlan 2019) and dam formation
375 process and the unsteadiness of the flow point out the need for a broader validation through a large set
376 and repetition of tests. Specific attention should be given to the physical properties of the debris dam,
377 including its porosity, geometry and temporal evolution. It is important to point out that the applicability
378 of these results is only limited to the tested hydraulic conditions, as different waves with different flow
379 velocities, water depths and durations might lead to different results in terms of dam formation,
380 hydrodynamic forces and cantilever arms.

381 In addition, Wüthrich et al. (2018a) pointed out some key differences in hydrodynamic behavior between
382 dry bed surges and wet bed bores, representing any subsequent tsunami wave. The influence of such
383 difference in the formation of the debris dam would be of interest for future work.

384 From a structural prospective, this study focused on relatively large building porosities ($P = 60\%$),
385 however smaller porosity values are most likely to influence the damming process. For these, stronger
386 separation lines around the building might reduce the debris volume retained by the structure, leading
387 to less hydrodynamic forces, yet making the building more vulnerable to peak impact forces. In addition,
388 lower blockage ratios might have a similar influence, showing that the issue of debris damming on free-
389 standing structures should be addressed as a 3D phenomenon.

390 **Conclusion**

391 Literature preliminary and punctually describes the effect of debris during wave loading of a building
392 with openings. However, “pure” water waves are inexistent during real events as incoming waves
393 transport a large amount of debris. This experimental study presents explorative results on the influence
394 of two type of debris (forest debris and shipping containers) on the loading process of unsteady tsunami-
395 like waves propagating on dry bed and impacting buildings with openings. Specifically, this focuses on
396 the post-peak hydrodynamic forces generated by the formation of a “debris-dam”. Results showed that:

- 397 • Debris transported with a dry bed surge change the impact dynamics of the wave, augmenting
398 upstream water depths, the impact forces (and thus the load on the building) as well as the impulse.
399 Reasons are (1) the instantaneous momentum exchange with heavy containers during the initial
400 impact phase, as well as (2) a reduction of the building porosity during a hydrodynamic flow phase.
- 401 • The unsteady, initially supercritical flow generated a highly turbulent surface roller on the upstream
402 side of the building, responsible for the creation of a debris dam. The streamlines around the building
403 generated the ejection of a number of debris during the hydrodynamic phase, thus reducing the
404 retention efficient of the dam and pointing out the 3-dimentional nature of the process.
- 405 • The instantaneous peak impact forces augmented herein by a factor of 2 for forest debris (*i.e.* logs)
406 to a factor 8-10 for shipping containers, as compared to the force maximum measured for “pure”
407 water waves (reference, Test 0) without debris.
- 408 • The augmentation of the force measured during the post-peak hydrodynamic phase was negligible
409 for the shipping containers. However, it became important for the forest debris because of its

410 relatively small porosity and interlocking nature. The formation of a “debris-dam” generated
411 average hydrodynamic force up to a factor of 2, as compared to the “pure” water waves (reference,
412 Test 0), corresponding to a reduction of the building porosity.

413 • Configurations with both type of debris showed that containers near the building generated larger
414 “debris dams” as these remain blocked within the “debris-dam”. On the contrary, the presence of
415 logs or poles near the building represents a way to reduce the peak impact forces exerted on the
416 building by the shipping containers. In addition, such disposition reduced the amount of volume
417 blocked in front of the building, generating smaller “debris-dams”. This points out that pre-existing
418 debris dams have the ability to reduce impact loads of larger pieces of debris for any subsequent
419 wave.

420 • The increase in impulse transferred to the building was related to the retained volume and to the
421 type of debris. The ability of forest debris to interlock generated a “debris-dam” in front of the
422 building, and thus higher post peak hydrodynamic forces and impulse. Within the tested hydraulic
423 conditions, forest debris were also responsible for higher cantilever arms compared to the shipping
424 containers alone, thus resulting into more severe tilting moments on the building.

425 This study provides basic results on the effect of debris damming on porous free-stranding buildings
426 under unsteady flow conditions. However, these results are exploratory and only based on a limited
427 number of repetitions, thus pointing out the need of further research for a better understanding of the
428 governing process.

429 **Acknowledgment**

430 The study was supported by the Swiss National Science Foundation (SNSF) [grant number
431 200021_149112/1 and 200021_149112/2].

432 **References**

433 Aghl, P., Naito, C. and Riggs, H. (2015). Estimation of demands resulting from inelastic axial impact of steel
434 debris. *Engineering Structures*, 82:11-21.

435 ASCE7-06 (2016). Minimum design loads for buildings and other structures. *ASCE/SEI 7-16*, Reston (VA) USA,
436 66 pages.

437 Bezzola, G. R., and Hegg, C. (2007). Ereignisanalyse Hochwasser 2005 [2005 Flood event analysis], *Report*,
438 Bundesamt für Umwelt & Eidgenössische Forschungsanstalt für Wald, Schnee und Landschaft, Bern, Switzerland
439 (in German).

440 Bocchiola, D., Rulli, M. and Rosso, R. (2008). A flume experiment on the formation of wood jams in rivers. *Water*
441 *Resources Research* 44(2):W02408.

442 Bullock, G., Obhrai, C., Peregrine, D., and Bredmose, H. (2007). Violent breaking wave impacts. part 1: Results
443 from large-scale regular wave tests on vertical and sloping walls. *Coastal Engineering*, 54(8):602-617.

444 Chanson, H. (2006). Tsunami surges on dry coastal plains: Application of dam break wave equations. *Coastal*
445 *Engineering Journal*, 48(04):355–370.

446 Chock, G., Robertson, I., Kriebel, D., Francis, M., Nistor, I., (2012). Tohoku Japan Tsunami of March 11, 2011 –
447 Performance of Structures. Report, *American Society of Civil Engineers ASCE*, 348 pages.

448 Derschum, C., Nistor, I., Stolle, J., and Goseberg, N. (2018). Debris impact under extreme hydrodynamic
449 conditions part 1: Hydrodynamics and impact geometry. *Coastal Engineering*, 141:24-35.

450 Dias, P., Dissanayake, R., and Chandratilake, R. (2006). Lessons learned from tsunami damage in Sri Lanka.
451 *Proceedings of the Institution of Civil Engineers-Civil Engineering*, 159(2):74–81.

452 FEMA55 (2000). *Coastal Construction Manual*. Federal Emergency Management Agency (FEMA), Chapter 8 -
453 Washington DC, USA, 82 pages.

454 Fritz, H.M., Petroff, C.M., Catalán, P.A., Cienfuegos, R., Winckler, P., Kalligeris, N., Weiss, R., Barrientos, S.E.,
455 Meneses, G., Valderas-Bermejo, C. and Ebeling, C., (2011). Field survey of the 27 February 2010 Chile tsunami.
456 *Pure and Applied Geophysics*, 168(11):1989-2010.

457 Furlan, P., Pfister, M., Matos, J., Amado, C., and Schleiss, A. J. (2018). Experimental repetitions and blockage of
458 large stems at ogee crested spillways with piers. *Journal of Hydraulic Research*, 1-13. (paper not yet assigned to
459 an issue)

460 Furlan, P. (2019). Blocking probability of large wood and resulting head increase at ogee crest spillways. *EPFL*
461 *PhD Thesis*, Lausanne, Switzerland.

462 Goseberg, N., Nistor, I., Mikami, T., Shibayama, T. and Stolle, J. (2016b). Non-intrusive Spatiotemporal Smart
463 Debris Tracking in Turbulent Flows with Application to Debris-Laden Tsunami Inundation. *Journal of Hydraulic*
464 *Engineering*, 142(12): 04016058.

465 Goseberg, N., Stolle, J., Nistor, N. and Shibayama, T. (2016a). Experimental analysis of debris motion due the
466 obstruction from fixed obstacles in tsunami-like flow conditions. *Coastal Engineering*, 118: 35-49.

467 Haehnel, R.B. and Daly, S.F. (2004). Maximum impact force of woody debris on floodplain structures. *Journal of*
468 *Hydraulic Engineering*, 130(2):112–120.

469 Jaffe, B. E., Goto, K., Sugawara, D., Richmond, B. M., Fujino, S., and Nishimura, Y. (2012). Flow speed estimated
470 by inverse modeling of sandy tsunami deposits: Results from the 11 March 2011 tsunami on the coastal plain near
471 the Sendai Airport, Honshu, Japan. *Sedimentary Geology*, 282:90-109.

472 Matsutomi, H., (2009). Method for estimating collision force of driftwood accompanying tsunami inundation flow.
473 *Journal of Disaster Research*, 4(6):435-440.

474 Naito, C., Cercone, C., Riggs, H. R., and Cox, D. (2013). Procedure for site assessment of the potential for tsunami
475 debris impact. *Journal of Waterway, Port, Coastal, and Ocean Engineering*, 140(2):223–232.

476 Nistor, I., Goseberg, N., Stolle, J., Mikami, T., Shibayama, T., Nakamura, R., and Matsuba, S. (2016).
477 Experimental investigations of debris dynamics over a horizontal plane. *Journal of Waterway, Port, Coastal, and*
478 *Ocean Engineering*, 143(3):04016022.

479 Nistor, I., Palermo, D., Cornett, A., Al-Faesly, T. (2011). Experimental and numerical modeling of tsunami loading
480 on structures. *Proceedings of 32nd Conference on Coastal Engineering*, Shanghai, China, 30 June-5 July

481 Nistor, I.; Goseberg, N.; Stolle, J. (2017) Tsunami-Driven Debris Motion and Loads: A Critical Review. *Frontiers*
482 *Built Environment*, 3(2):1-11.

483 Parola, A.C. (2000). Debris Forces on Highway Bridges; *Transportation Research Board*: Washington, DC, USA.

484 Pasha, G.A. and Tanaka, N. (2016) Effectiveness of Finite Length Inland Forest in Trapping Tsunami-Borne Wood
485 Debris. *Journal of Earthquake and Tsunami*, 10(4): 1650008.

486 Pfister, M., Capobianco, D., Tullis, B., and Schleiss, A. J. (2013). Debris-blocking sensitivity of piano key weirs
487 under reservoir-type approach flow. *Journal of Hydraulic Engineering*, 139(11):1134-1141.

488 Ritter, A. (1892). Die Fortpflanzung der Wasserwellen. *Zeitschrift Verein Deutscher Ingenieure*, 36(33):947-954.

489 Robertson, I., Riggs, H.R., Yim, S.C. and Young, Y.L. (2007). Lessons from Hurricane Katrina storm surge on
490 bridges and buildings. *Journal of Waterway, Port, Coastal and Ocean Engineering*, 133(6):463-483.

491 Rueben, M., Cox, D., Holman, R., Shin, S., Stanley, J., (2015). Optical measurements of tsunami inundation and
492 debris movement in a large-scale wave basin. *Journal of Waterway, Port, Coastal and Ocean Engineering*,
493 141(1):04014029

494 Saatcioglu, M., Ghobarah, A. and Nistor, I. (2005) Effects of the December 26, 2004 Sumatra earthquake and
495 tsunami on physical infrastructure. *Journal of Earthquake. Technology*, 42(4): 79-94.

496 Schmocker, L., and Hager, W. H. (2013). Scale modeling of wooden debris accumulation at a debris rack. *Journal*
497 *of Hydraulic Engineering*, 139(8):827-836.

498 Shafiei, S., Melville, B.W., Shamseldin, A.Y., Beskhyroun, S., and Adams, K.N. (2016). Measurements of
499 tsunami-borne debris impact on structures using an embedded accelerometer. *Journal of Hydraulic Research*,
500 54(4):435-449.

501 Stolle, J., Derschum, C., Goseberg, N., Nistor, I. and Petriu, E. (2018a). Debris impact under extreme
502 hydrodynamic conditions part 2: Impact force responses for non-rigid debris collisions. *Coastal Engineering*,
503 141:107-118

504 Stolle, J., Goseberg, N., Petriu, E., Nistor, I. (2018c). Probabilistic Investigation and Risk Assessment of Debris
505 Transport in Extreme Hydrodynamic Conditions. *Journal of Waterways, Port, Coastal, and Ocean Engineering*,
506 144(1):04017039-1.

507 Stolle, J., Nistor, I., Goseberg, N., Mikami, T., Shibayama, T. (2017). Entrainment and Transport Dynamics of
508 Debris in Extreme Hydrodynamic Conditions. *Coastal Engineering Journal*, 59(3):1750011.

509 Stolle, J., Takabatake, T., Mikami, T., Shibayama, T., Goseberg, N., Nistor, I., and Petriu, E. (2017). Experimental
510 Investigation of Debris-Induced Loading in Tsunami-Like Flood Events. *Geosciences*, 7(3):74

511 Stolle, J., Takabatake, T., Nistor, I., Mikami, T., Nishizaki, S., Hamano, G., Ishii, H., Shibayama, T., Goseberg,
512 N., Petriu, E. (2018b). Experimental investigation of debris damming loads under transient supercritical flow
513 conditions. *Coastal Engineering*, 139:16-31.

514 Takahashi, S., Sugano, T., Tomita, T., Arikawa, T., Tatsumi, D., Kashima, H., Murata, S., Matsuoka, Y., and
515 Nakamura, T. (2010). Joint survey for 2010 Chilean earthquake and tsunami disaster in ports and coasts. *PARI*
516 *Technical Note 1224*, Port and Airport Research Institute, Kuriyama, Japan.

517 Triatmadja, R., and Nurhasanah, A. (2012). Tsunami force on buildings with openings and protection. *Journal of*
518 *Earthquake and tsunami*, 6(4):1250024.

519 Wüthrich, D. (2018). Extreme Hydrodynamic impact onto buildings. *EPFL PhD Thesis* (N. 8116). Lausanne,
520 Switzerland, 245 pages.

521 Wüthrich, D., Pfister, M. Nistor, I. and Schleiss, A.J. (2018a). Experimental Study of Tsunami-Like Waves
522 Generated with a Vertical Release Technique on Dry and Wet Beds. *Journal of Waterways, Port, Coastal and*
523 *Ocean Engineering*, 144(4):04018006.

- 524 Wüthrich, D., Pfister, M., Nistor, I. and Schleiss, A.J. (2018b). Experimental study on forces exerted on buildings
525 with openings due to extreme hydrodynamic events. *Coastal Engineering*, 140:72-86.
- 526 Yeh, H., Barbosa, A. and Mason, B.H., (2015). Tsunamis effects in man-made environment. *Encyclopedia of*
527 *complexity and systems science*, pp.1-27.
- 528 Yeom, G., Nakamura, T., and Mizutani, N. (2009). Collision analysis of container drifted by run-up tsunami using
529 drift collision model. *Journal of Disaster Research*, 4(6):441–449.
- 530